Supporting Information

Gordo *et al.* 10.1073/pnas.0805658105

SI Text

General Considerations. All reactions were carried out under argon with dry solvents unless otherwise noted. All commercially available reagents were used without further purification. The solvents were dried and distilled. A Dowex ion exchange resin (ACROS) was used for chloride anions exchange on **1**.

Chromatography. Reactions were monitored by TLC performed on DC-Fertigplatten SIL G-25 UV_{254} (Macherey-Nagel GmbH) or by analytical high-performance liquid chromatography with a RP-C_{18} column (Symmetry300 C18 5 μm 4.6 × 150 mm) on a high-performance liquid chromatograph (HPLC; Agilent Technologies Series 1200 with UV detection). Semipreparative-HPLC purification was performed on Waters HPLC 600 equipment with a quaternary pump (0.01–20 ml/min). Standard column chromatography was done on silica gel by SDS (chromagel 60 ACC, 40–60 mm) following the procedure described by Still (1).

Analysis. Yields refer to chromatographically pure compounds. ^{1}H NMR and ^{13}C NMR spectra were recorded on Bruker Avance 400 UltraShield spectrometer (^{1}H, 400 MHz; ^{13}C, 100 MHz) and are reported in parts per million relative to the residual solvent peak. Data for ^{1}H are reported as follows: chemical shift (δ ppm), multiplicity (s = singlet, d = doublet, m = multiplet), coupling constant in hertz, and integration. Exact masses were measured on a Waters LCT Premier liquid chromatograph coupled time-of-flight mass spectrometer (HPLC/MS-TOF) with electrospray ionization (ESI). Melting points were measured with a Büchi B-540 apparatus.

5,11,17,23-Tetraguanidinemethyl-25,26–27,28-biscrown-3-calix[4]-arene tetrahydrochloride (1). Boc-protected compound **3** (50 mg, 0.03 mmol) was dissolved in 0.6 ml of 4 M HCl (2.4 mmol) in 1,4 dioxane (1.00 mmol per Boc group), under inert atmosphere. The solution was stirred for 24 h at room temperature.

After evaporation of the solvent, the residue was triturated in AcOEt. The resulting solid was purified by semipreparative HPLC (100 μl of a 37.5 mg/ml solution injected in a Waters SymmetryC_{18} 500 Å 10 × 150 mm semipreparative column, and eluted with a 5–35% gradient of acetonitrile in water with 0.05% TFA along 20 min, flux: 4.7 ml/min). Pure compound eluted at 16.2 min with a final yield of 50%. Anion exchange to chloride yielded the tetrahydrochloride salt **1**.

^{1}H NMR (400 MHz, CD_3CN): δ 7.08 (s, 8H, ArH), 5.03 (d, J = 12.1 Hz, 2H, ArCH*Hax*Ar), 4.48 (d, J = 12.1 Hz, 2H, ArCH-*Hax*Ar), 4.28–4.23 (m, 12H, CH_2O), 4.13 (d, J = 6.2 Hz, 8H, CH_2Gua), 3.74–3.69 (m, 4H, CH_2O), 3.28 (d, J = 12.3 Hz, 2H, ArCH*Heq*Ar), 3.21 (d, J = 12.3 Hz, 2H, ArCH*Heq*Ar).

^{13}C NMR (100 MHz, CD_3CN): δ 157.3 (CAr *ipso*), 154.8 (CGua), 135.9 (CAr *para*), 132.0 (CAr *orto*), 129.9 (CHAr *meta*), 128.1 (CHAr *meta*), 76.7 (CH_2O), 74.4 (CH_2O), 43.3 (CH_2Gua), 29.7 (ArCH_2Ar), 29.0 (ArCH_2Ar).

Exact mass (ESI+) m/z of [M − Cl^-]$^+$ calc.: 957.3867 uma, found: 987.3824.

m.p.: >330°C.

5,11,17,23-Tetraminomethyl-25,26–27,28-biscrown-3-calix[4]arene tetrahydrochloride (2). To a stirred solution of tetracyano calixarene **4** (0.60 mmol) in 52 ml of dry THF at 0°C, 18 ml (18 mmol) of a BH_3 solution (1 M in dry THF) were added. The reaction mixture was heated in a sealed tube under nitrogen for 24 h, then 5 ml of MeOH and 15 ml of 1 N HCl were added (CAUTION!) and the mixture heated at 50°C for 0.5 h. THF was removed under reduced pressure. To the remaining aqueous phase was added another 10-ml amount of 1 N HCl and several washes with CH_2Cl_2 (3 × 15 ml) were performed. Finally, the aqueous solvent was removed under reduced pressure and the remaining residue was triturated in AcOEt and filtered. The chloride salt of compound **3** was obtained with 80% yield.

^{1}H NMR (400 MHz, CD_3OD): δ 6.93 (s, 8H, ArH), 4.92 (d, J = 12.8 Hz, 2H, ArCH*Hax*Ar), 4.40 (d, J = 12.7 Hz, 2H, ArCH-*Hax*Ar), 4.23–4.14 (m, 8H, OCH_2), 3.80–3.73 (m, 8H, OCH_2), 3.56 (s, 8H, CH_2N), 3.21 (d, J = 12.7 Hz, 2H, ArCH*Heq*Ar), 3.15 (d, J = 12.8 Hz 2H, ArCH*Heq*Ar), 2.85 (bs, 8H, NH_2).

^{13}C NMR (100 MHz, CD_3OD): δ 155.4 (CAr *ipso*), 136.7 (CAr *para*), 135.4 (CAr *ortho*), 129.7 (CAr *meta*), 128.8 (CAr *meta*), 77.4 (OCH_2), 75.7 (OCH_2), 55.4 (CH_2N), 30.5 (ArCH_2Ar).

MS ESI(+) m/z: 717.3 [M − $3Cl^-$]$^+$.

m.p.: >330°C.

5,11,17,23-Tetrakis(*N,N′*-bis-*tert*-butoxycarbonyl)guanidinemethyl-25,26–27,28-biscrown-3-calix[4]arene (3). To a solution of aminomethylcalix[4]arene (**2**) (0.108 g, 0.16 mmol) and triethylamine (0.088 ml, 0.63 mmol) in 1.5 ml of dry CH_2Cl_2, *N,N′*-bis-(*tert*-butoxycarbonyl)guanidine *N″*-triflate **8** (0.249 g, 0.63 mmol), dissolved in 1.5 ml of dry CH_2Cl_2, was added under inert atmosphere. The reaction was stirred at room temperature for 36 h and quenched with 1 N HCl (2 × 2 ml), water (1 × 2 ml), and brine (1 × 2 ml). After drying, the solvent was removed under reduced pressure. Finally, compound **3** was purified by flash column chromatography on silica gel eluting with Et_2O:Hex (1:4). **3** was obtained as a colorless solid in a 48% yield.

^{1}H NMR (400 MHz, $CDCl_3$): δ 8.38 (s, 4H, NHBoc), 6.88 (d, J = 5.0 Hz, 8H, ArH), 4.90 (d, J = 12.3 Hz, 2H, ArCH*Hax*Ar), 4.39–4.27 (m, 10 H, ArCH*Hax*Ar, OCH_2), 4.19–4.13 (m, 12H, OCH_2, CH_2Gua, ArCH*Hax*Ar), 3.79–3.73 (m, 4H, CH_2O), 3.16 (d, J = 11.7 Hz, 2H, ArCH*Heq*Ar), 3.11 (d, J = 12.3 Hz, 2H, ArCH*Heq*Ar), 1.41 (d, J = 10.5 Hz, 36H, $C(CH_3)_3$).

^{13}C NMR (100 MHz, $CDCl_3$): δ 163.6 (CO), 155.7 (CGua), 154.79 (CGua), 153.1 (CAr *ipso*), 135.7 (CAr *para*), 135.5 (CAr *para*), 132.1 (CAr *orto*), 128.6 (CHAr *meta*), 127.6 (CHAr *meta*), 83.0 ($C(CH_3)_3$), 79.1 (OCH_2), 74.8 (OCH_2), 45.0 (CH_2Gua), 30.8 (ArCH_2Ar), 30.0 (ArCH_2Ar), 28.3 ($C(CH_3)_3$), 28.1 ($C(CH_3)_3$).

Exact Mass (ESI) m/z [M + $3Cl^-$]$^+$: calc.: 1649.8713, found: 1649.8678.

m.p.: >330°C.

Synthesis. See Fig. S3. For molecular dynamics, see Figs. S1 and S2. For biophysical characterization, see Figs. S4–S9.

1. Still WC, Kahn M, Mitra AJ (1978) Rapid chromatographic technique for preparative separations with moderate resolution. *J Org Chem* 43:2923–2925.
2. Arduini A ,*et al.* (1995) Calix[4]arenes blocked in a rigid cone conformation by selective functionalization at the lower rim. *J Org Chem* 60:1454–1457.
3. Feichtinger K, Zapf C, Sings HL, Goodman M (1998) Diprotected triflylguanidines: a new class of guanidinylation reagents. *J Org Chem* 63:3804–3805.
4. Mayer M, Meyer B (2001) Group epitope mapping by saturation transfer difference NMR to identify segments of a ligand in direct contact with a protein receptor. *J Am Chem Soc* 123:6108–6117.
5. Hinshelwood J, Perkins SJ (2000) Conformational changes during the assembly of Factor B from its domains by 1H NMR spectroscopy and molecular modelling: their relevance to the regulation of Factor B activity. *J Mol Biol* 301:1267–1285.

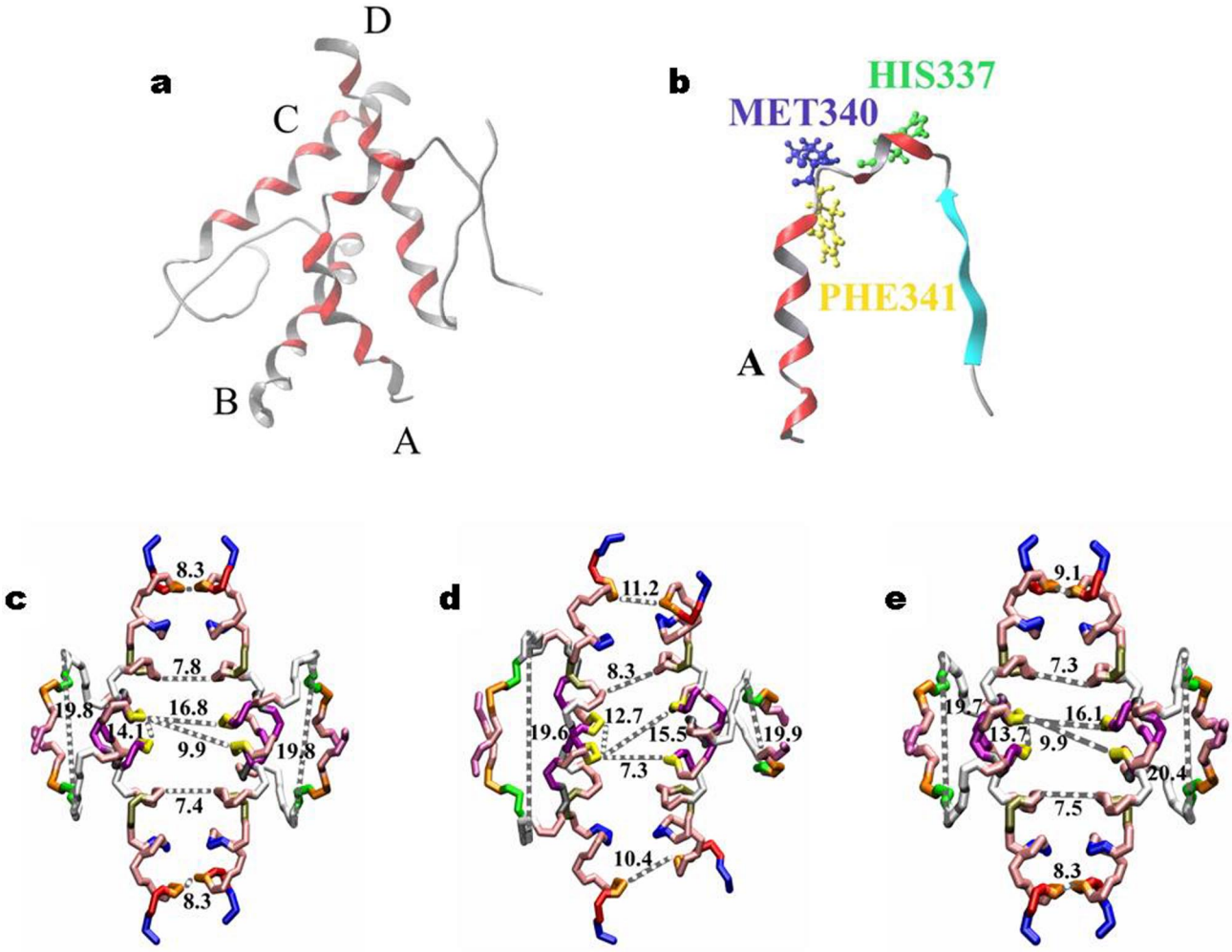

Fig. S1. Protein structures from molecular dynamics. Examples of the most disrupted tetrameric structure (*a*) and the most disturbed monomer from p53TD-R337H simulation at 400 K (*b*). (*c*–*e*) Representative structures. The atom coordinates obtained from the trajectories were grouped into classes of similar structures. Distances between couples of structures obtained at different times were determined by measuring backbone rmsd between them after fitting. Each structure was added to a specific cluster when the distance to any of its elements to the cluster was less than a 0.75-Å cutoff. Each cluster was represented by an average structure. The analysis was carried out with the g_cluster tool in Gromacs. At 300 K, only one representative structure of the mutant protein was found (*c*), whereas at 400 K, 27 different altered structures do exist (*d*). (*e*) At 400 K, but in the presence of calixarene, a unique representative structure was found, similar to that at standard conditions.

Fig. S2. Trajectories of the most relevant distances for tetramer integrity. (*a*) Hydrogen bond distances relevant for the tetramer. Minimum distances between the atoms involved in the interaction were analyzed for the following residue pairs: Gln-331-Asn-345; Arg/His-337-Asp-352; Arg-333-Asp-352; Arg/His-337-Asn-345; Arg/His-337-Glu-349; and Arg-333-Glu-349 in the trajectories of the wild-type protein, the mutant protein, and the mutant protein plus ligand at 400 K. (*b*) Distances between hydrophobic residues relevant for the tetramer. Minimum distances between the closest atoms in side chains of those residues intervening in hydrophobic packing: Ile-332_A-Arg-337_A; Ile-332_A-Phe-341_A; Arg/His-337_A-Met-340_A; Arg/His-337_A-Phe-341_A; Met-340_A-Phe-341_A; Ile-332_A-Leu-330_D; Phe-341_A-Phe-341_D; and Leu-330_D-Phe-341_D in the trajectories of the wild-type protein, the mutant protein, and the mutant protein plus ligand at 400 K. All of the distances measured from the simulation of the mutant protein in the presence of ligands showed equal to those in the wild-type protein (pink traces superposing to blue traces in the plots). The analysis was performed with the Gromacs tool g_mindist. In general, the pink traces representing the mutant protein plus ligand do not superpose to the blue traces representing the wild-type protein but are closer to the magenta traces, corresponding to the mutant protein alone. Thus, the bond interactions lost in p53TD-R337H in the absence of ligand were not maintained in the presence of calixarene.

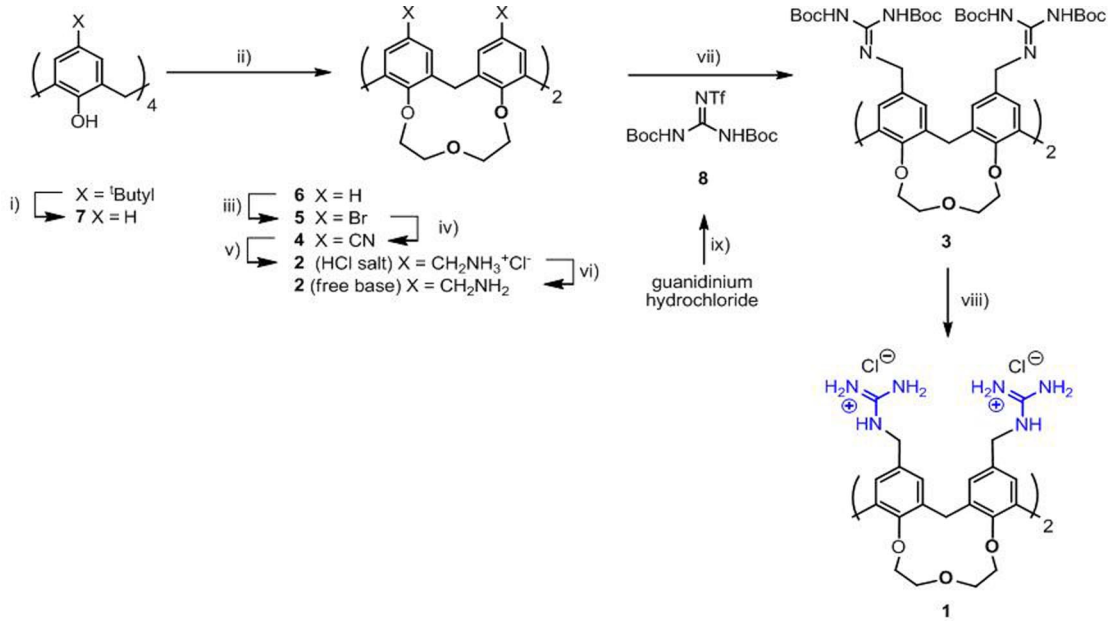

Fig. S3. Synthesis of ligands **1** and **2**. Reagents and conditions: (*i*) $AlCl_3$, phenol, toluene, 24°C, 24 h (81%). (*ii*) $(TsOCH_2CH_2)_2O$, NaH, DMF, 24°C, 4 h (41%). (*iii*) NBS, DMF, 24°C, 24 h (90%). (*iv*) CuCN, NMP, 200°C, MW, 15 min (48%) (2). (*v*) 1 M BH_3-THF, sealed tube, reflux, 24 h (88%) (2). (*vi*) Extraction of **2** (free base) in CH_2Cl_2 from 1 N NaOH solution of **2** (HCl salt) (quant.). (*vii*) 8 (3), Et_3N, CH_2Cl_2, 24°C, 24 h (45%). (*viii*) 4 N HCl in 1,4-dioxane, 24°C, 24 h, semiprep. HPLC purification (gradient: 0–35% CH_3CN in H_2O + 0.05% CH_3COOH in 20 min, 4.7 ml/min), chloride anion exchange on **1** (50%). (*ix*) (*a*) NaOH, $(Boc)_2O$, 1,4-dioxane, 0→24°C, 24 h (50%); (*b*) Triflic anhydride, Et_3N, −78→24°C, 5 h (82%).

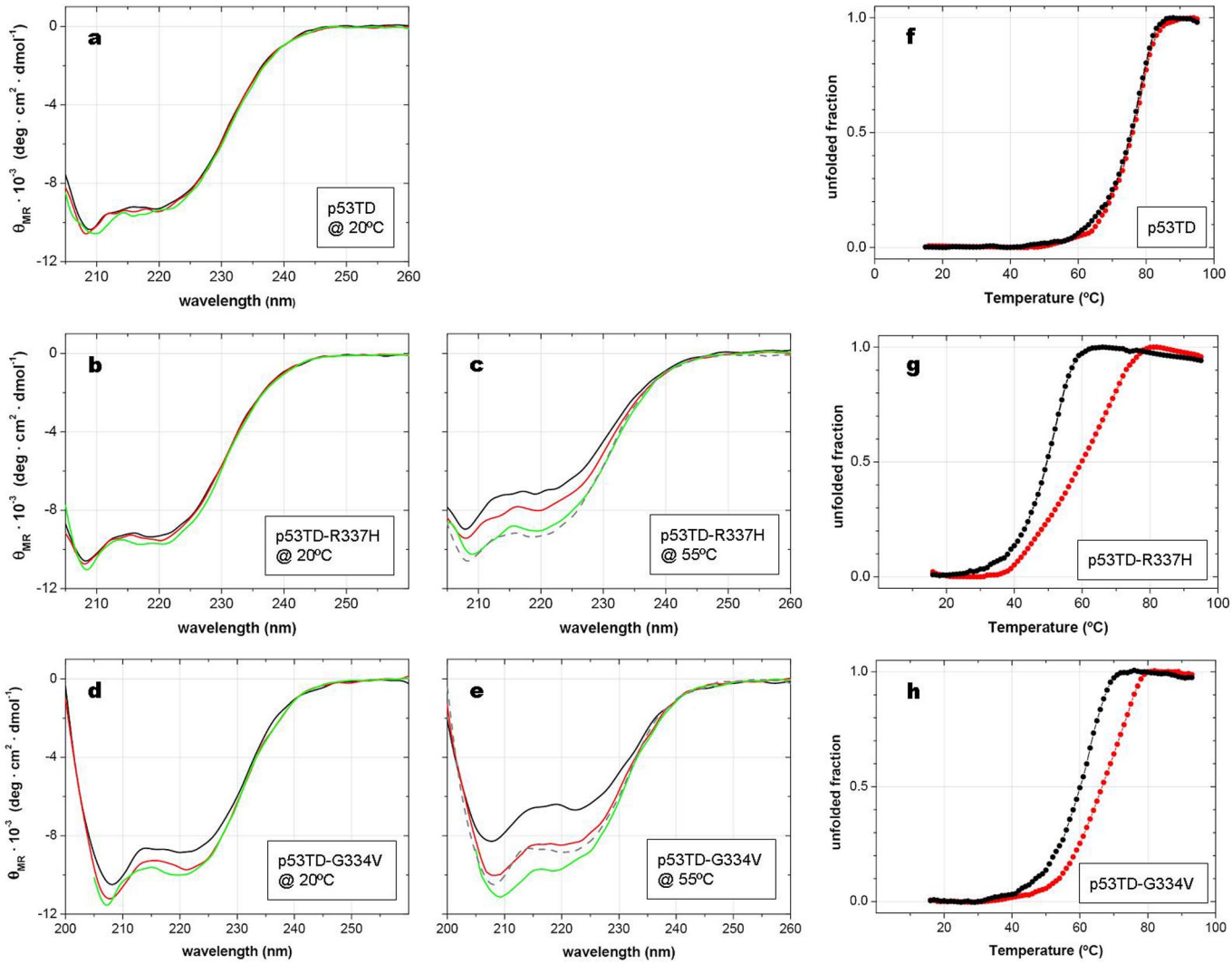

Fig. S4. Ligand **1** evaluated by circular dichroism. Effects of ligand **1** on protein secondary structure. (*a*) Ligand addition did not modify the circular dichroism spectra of p53TD (30 μM monomer) at 20°C: free protein (black trace), in the presence of 60 μM (red) and 120 μM (green) of ligand **1**. For the mutant protein p53TD-R337H (*b*), under the same conditions, no clear change on the CD spectra could be detected either. However, structural stabilization promoted by **1** binding was observed at 55°C (*c*). For mutant p53TD-G334V, changes are more evident, at both room temperature (*d*) and 55°C (*e*), thus suggesting the stabilization of a more structured species (i.e., the tetramer). Dashed gray lines in *c* and *e* correspond to the CD spectra for the free proteins at 20°C. The thermal stability was also detected by the CD unfolding curves for 10 μM (monomer) of p53TD (*f*), p53TD-R337H (*g*), and p53TD-G334V (*h*), in the absence (black trace) and in the presence of 20 μM ligand **1** (red trace). These results perfectly agree with the shifts observed by differential scanning calorimetry (see main text). Whereas the wild-type p53TD was basically unperturbed, the unfolding profile of mutant p53TD-R337H was asymmetrically distorted as would correspond to the biphasic denaturation of the ligand-free (low-temperature side) and the ligand-bound (high-temperature side) forms of the mutant. For p53TD-G334V the transition shift is more moderate and monophasic. Reproducibility of the results by different techniques using very different concentrations (i.e., 10 μM by CD and 100 μM by DSC) proved the specificity of the induced thermal stabilization. CD experiments were recorded in a Jasco J-810 spectropolarimeter, equipped with a Jasco-CDF-426S Peltier thermostated cell holder and a Julabo external bath. Samples were prepared in water and the pH was thoroughly adjusted to 7.0. Each CD spectrum was obtained by averaging three or five scans, recorded at 10 nm·min^{-1}, by using a 1-mm path length quartz cell. For the thermal denaturation curves, samples were heated from 15°C to 95°C at 1.5°C·min^{-1} in a 10-mm path length quartz cell. Ellipticity changes at 220 nm were measured and used to calculate the apparent molar fraction of denatured molecules (*y* axis) at each temperature (*x* axis), assuming a two-state unfolding model. For clarity, experimental data were smoothed by using the software package provided by Jasco.

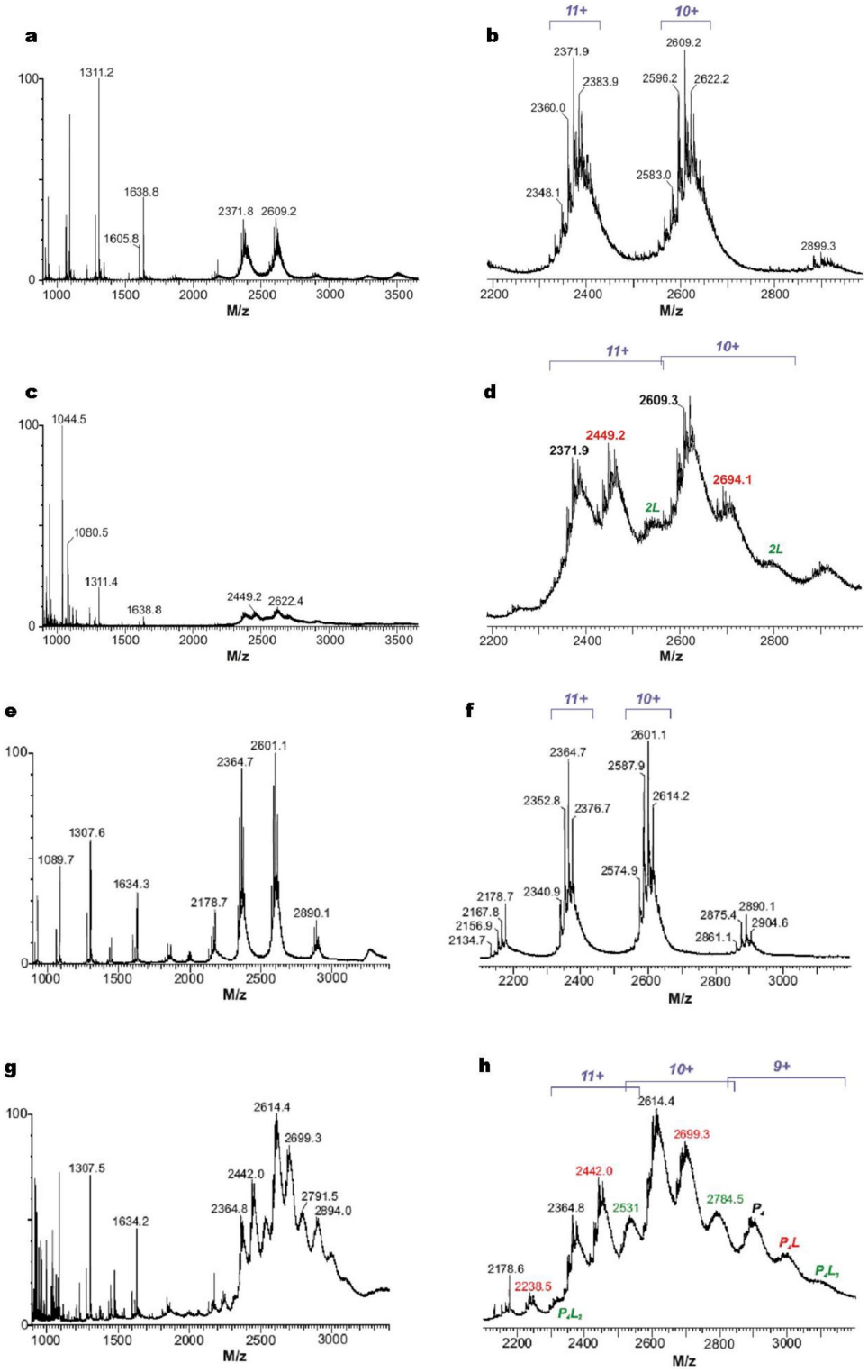

Fig. S5. Noncovalent tetrameric protein–ligand complexes detected by ESI-MS. Masses labeled in black correspond to the free protein; in green, those from the single-bound complex; and in red, the double-bound complex. The charge state of the tetramer is indicated above the peaks. *a* and *b* correspond to 12.5 μM p53TD (tetramer) in 10 mM NH_4Cl at pH 7.0, and *c* and *d* correspond to p53TD with 125 μM of compound **1** added. *e* and *f* correspond to 12.5 μM p53TD-R337H (tetramer) in 10 mM NH_4Cl at pH 7.0, and *g* and *h* correspond to p53TD-R337H with 125 μM **1** added. ESI-MS measurements were performed in a Synapt HDMS mass spectrometer (Waters) equipped with a NanoMate automated nanoelectrospray sample dispenser (Advion BioSciences). The spray voltage was set to 1.7 kV and the delivery pressure at 0.3 psi. The mass detection was carried out in positive mode at the source, at 80°C for wild-type p53TD and 20°C for p53TD-R337H. The sampling cone voltage was 70 mV, and the collision energy in the trap and the transfer was set to 10.

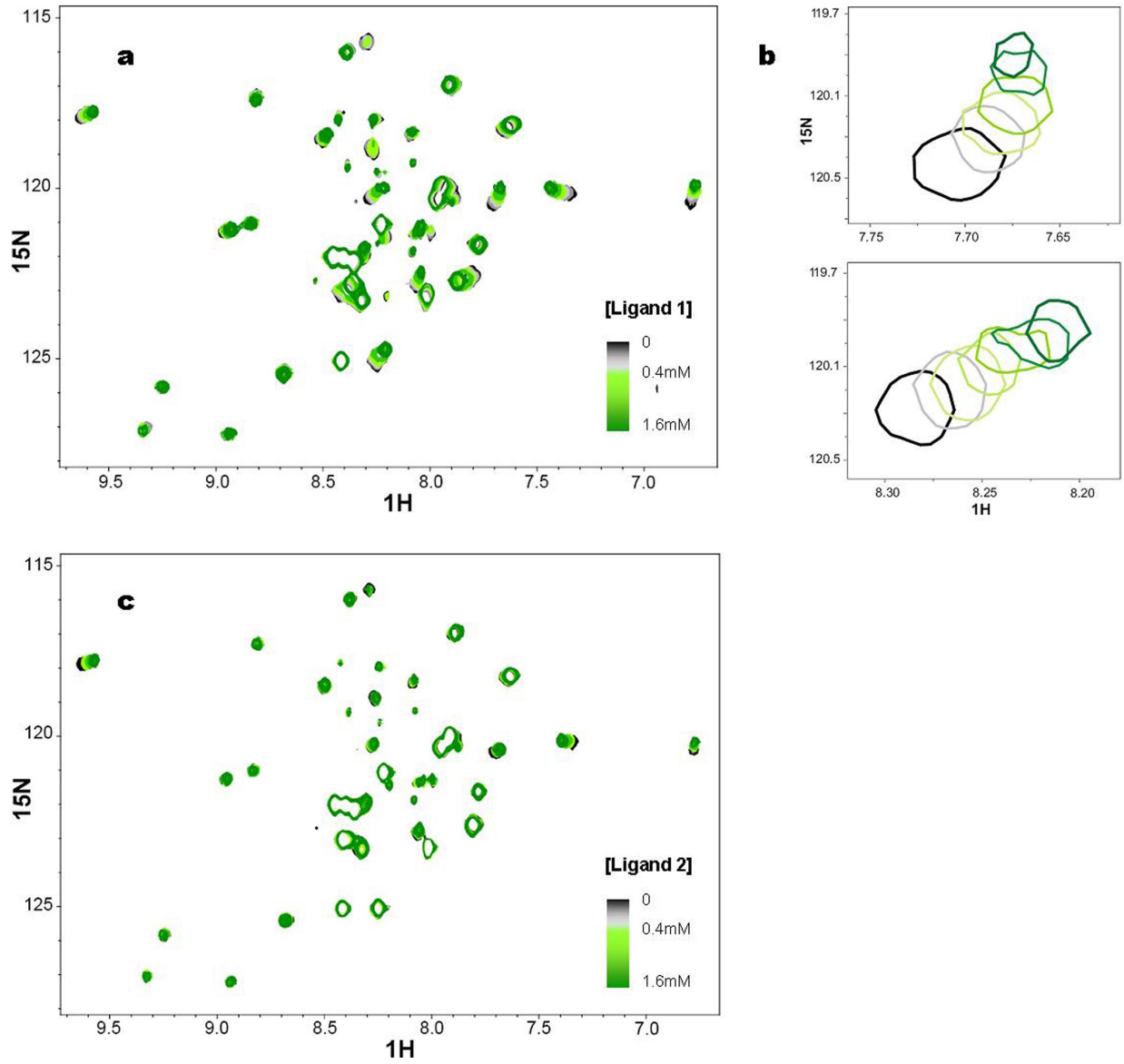

Fig. S6. p53TD-G334V titration with ligands **1** and **2**. Overlapped ^{1}H-^{15}N-HSQC spectra for the titration of 100 μM (tetramer) ^{15}N-p53TD-G334V with ligand **1** (*a*) and control ligand **2** (*c*), in water (10% D_2O) pH 7.04 at 25°C. Free protein is shown in black; ligand concentrations $<$400 μM are in the gray scale; and those between 400 μM and 1.6 mM are in the green scale. (*b*) During the titration with ligand **1**, protein resonances did not evolve linearly but displayed a slight curvature, thereby suggesting the sequential binding of two molecules of ligand.

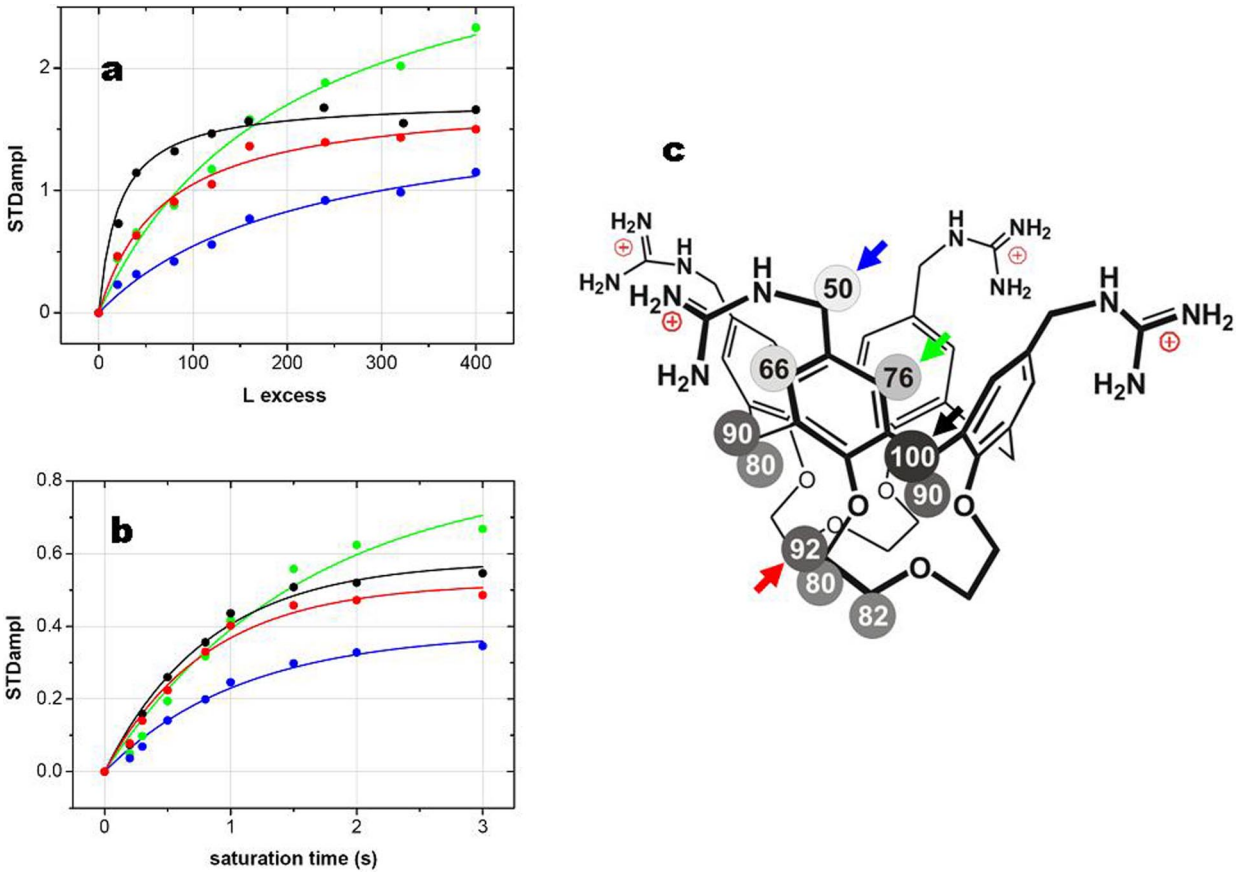

Fig. S7. ^{1}H saturation transfer difference (STD) experiments on ligand **1**. (*a*) Curves show the saturation of the STD effect at increasing ligand excesses, which is a striking experimental evidence of the specificity (4) of the interaction between p53TD and ligand **1**. The ligand titration was carried out at 283 K in a convergent manner, in a sample in D_2O containing 3.75 μM (tetramer) p53TD; the ligand excesses plotted in *a* correspond to ligand-to-tetramer molar ratios. The STD amplification factors (STDampl) were adjusted to a saturation curve as a function of the ligand concentration: $STD = (STD_{MAX}[L]_T)/(K_D + [L]_T)$. Only four representative protons are displayed, which are color labeled in *c*. Because of the significantly marked differences in the longitudinal relaxation of ligand **1** protons, the build-up curves were constructed for a reliable epitope mapping. In *b*, the STD build-up curves for individual protons presenting different saturation degrees and relaxation times are plotted (the color code is indicated in *c*.)

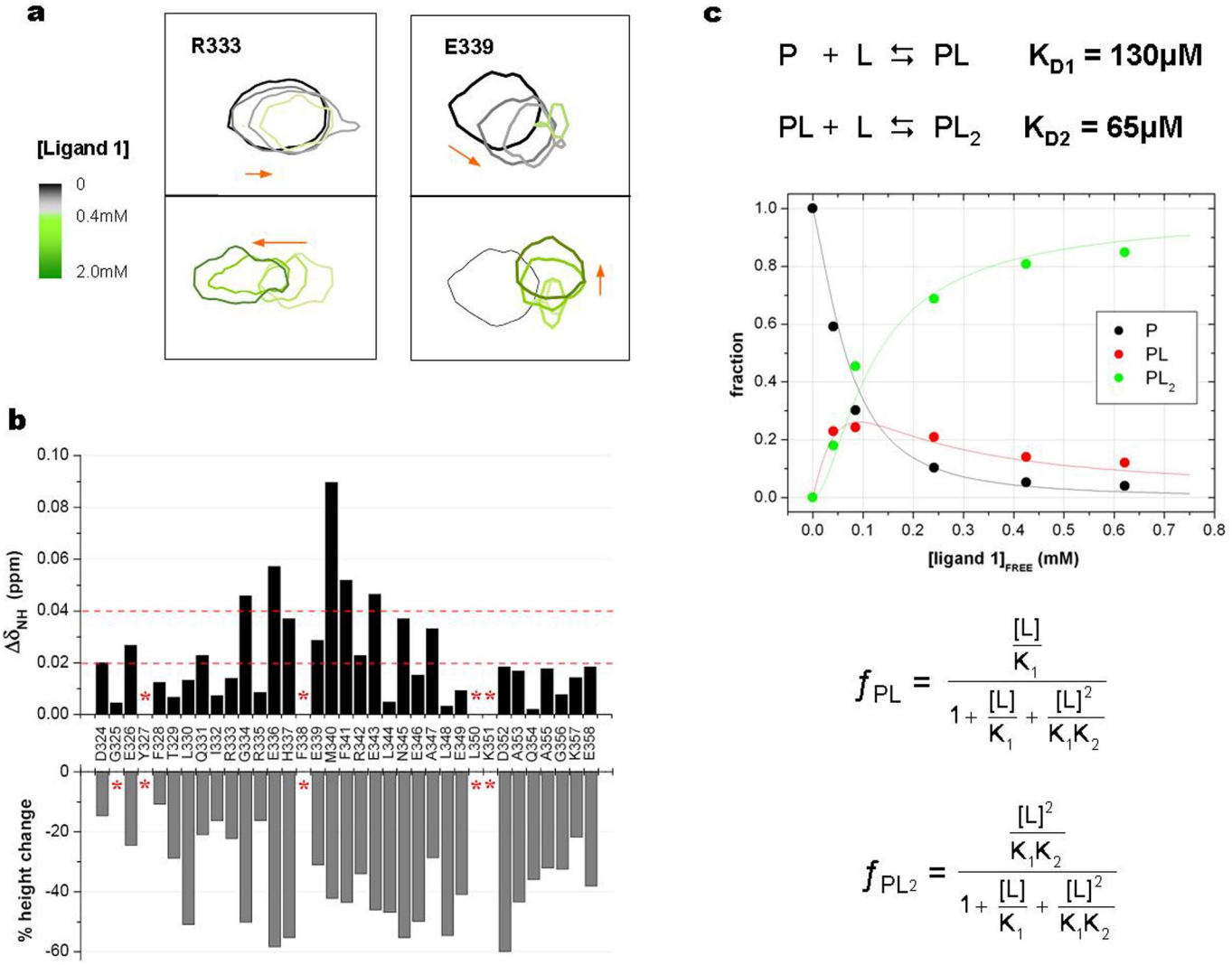

Fig. S8. Two stages of the interaction of ligand **1** with p53TD-R337H. (*a*) Detail of the evolution of the ^{1}H-^{15}N-HSQC resonances R333 and E339 of mutant protein p53TD-R337H on titration with ligand **1**. For clarity, the two different stages have been separated: *Upper* for the first stage (up to 0.4 mM ligand) and *Lower* for the second stage (from 0.4 to 2 mM). Shifting was accompanied by broadening. In fact, final resonances were never as sharp as the free-protein ones. This was in agreement with the existence of a dynamic binding event, and further suggested structural rearrangements of the protein. Resonances within the binding pocket disappeared at the end of the first stage and reemerged elsewhere; this change also supported the induction of structural rearrangement in the protein on ligand binding. Loss of the resonance traces made impossible the mapping of the protein at the end of the titration. However, it was possible to map changes during the first stage. (*b*) Representation of the shift and the decrease in peak height for the resonances of R337H in the presence of 0.2 mM ligand. As expected, the more sensitive residues were those within the binding site (*, undetermined data). (*c*) The populations for the free protein and the ligand-bound species were determined according to the intensity of the resonances and its shift (dots in the graphic), and those experimental values were fitted to the theoretical equations for a sequential binding (lines in the graphic), resulting in K_{D1} = 130 μM and K_{D2} = 65 μM.

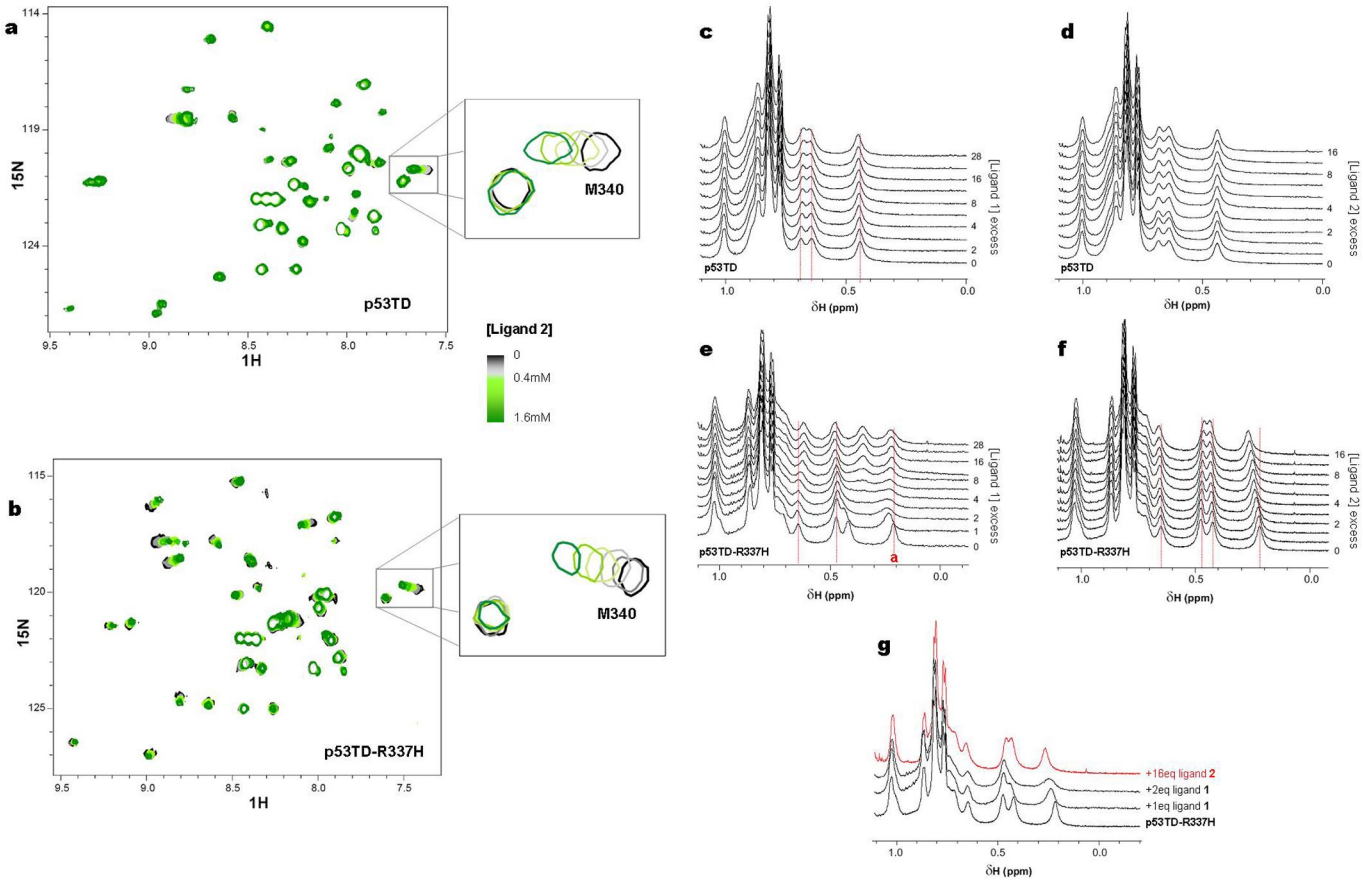

Fig. S9. Comparison of the changes induced in the NMR spectra on addition of ligand **1** and control ligand **2**. Overlapped ^{1}H-^{15}N-HSQC spectra for the titration of ^{15}N-p53TD (*a*) and ^{15}N-p53TD-R337H (*b*) at 100 μM (tetramer) with control ligand **2**, in water (10% D_2O) pH 7.04 at 25°C. Free protein is shown in black, with 200 μM ligand in gray, and with 400 μM, 800 μM, and 1.6 mM in the green scale. Mathematical adjustment of the shifts in M340 resonance for wild-type p53TD (see *Methods*), resulted in a dissociation constant, K_D, $\approx$0.92 $\pm$ 0.06 mM, three times higher than that for ligand **1**, thus emphasizing the role of the guanidinium groups in the molecular recognition event. For p53TD-R337H, the unidirectional shift on M340 resonance was adjusted to a mathematical model considering that only one molecule of ligand interacted per tetramer, resulting in a $K_D \approx 0.6 \pm 0.1$ mM, considerably larger than that for ligand **1**. (*a* and *b*) Shown is the protein upfield methyl resonance evolution on titration with the calixarene ligands. The ^{1}H upfield region is very sensitive to protein conformational changes (5). Although for p53TD the presence of ligand B (*c*) or ligand B (*d*) did not make any difference, for mutant p53TD-R337H (*e*, *f*) nice changes on some of the resonances were clearly appreciated. Moreover, the trend of the p53TD-R337H upfield resonances correlated well with the detected by HSQC; the one-dimensional spectra enable us to better distinguish the two stages for the mutant titration with ligand **1**, and also show that ligand **2** changes were similar to the first stage of **1** (*e*). The broadness of the resonances at the end of ligand **1** titration correlated well, not only with the existence of dynamic binding events in an intermediate exchange rate, but also with the protein undergoing structural rearrangements on binding.